(Received 11 March 2025, Accepted 21 April 2025, Scheduled 4 May 2025)

Design of a Compact Dual-Band Metamaterial Bandpass Filter Using Multi-Type Fractal Geometries

Hayder S. Ahmed* and Aqiel N. Almamori

Electronic and Communications Department, Engineering College, University of Baghdad, Iraq

ABSTRACT: In this paper, a compact Dual-Band Bandpass Filter (BPF) has been proposed and designed based on two concepts. Firstly, transmission lines (TLs) feed the center resonators (CRs), which resonate at 11 GHz, while the metamaterial-based Center Resonators (CRs) resonate at 6 GHz for RF/Microwave applications. To miniaturize the planer structure, two different types of fractal geometry have been applied. First iteration modified-Minkowski fractal geometry has been applied on the CRs while the meander line with second order has been applied on the TLs. The proposed structure has been designed by using a Rogers RO4003 substrate with a thickness of 1.5 mm and a dielectric constant of 3.5. The simulation is implemented using CST microwave studio. To validate the proposed structure, the compact dual-band BPF is fabricated, and the measurements show high agreement with the simulation. Finally, the proposed structure achieves a 26% reduction compared to the previous work.

1. INTRODUCTION

The rapid advancement of wireless communication technologies has fueled a growing demand for compact, high-performance radio frequency (RF) and microwave components. In recent years, the Federal Communications Commission (FCC) has expanded unlicensed spectrum use between 5.925 GHz and 7.125 GHz [1], facilitating the deployment of Wi-Fi 6E, laying the groundwork for Wi-Fi 7, and supporting the expansion of the Internet of Things (IoT). Additionally, the 11 GHz band is primarily allocated for point-to-point radio communications. Therefore, reducing the size of electronic components is essential for improving efficiency in modern systems, reducing manufacturing costs, and enabling integration into modern wireless devices. As frequency bands become more crowded, and multifunctionality is required, compact circuit designs are essential to optimize performance while maintaining low insertion losses and high selectivity.

In the last two decades, the communication system has upgraded rapidly. One of the interests of researchers is the designation of compact communication systems. First, the authors designed multiband devices to make one device work in multi-applications [2–7]. The key to miniaturization is using fractal geometry. The objective of using fractal geometry is to increase the surface current path length. Consequently, a reduced resonant frequency or a reduced resonator size is required to maintain the design frequency [8]. Many researchers applied different fractal geometries to design different compact devices, such as Minkowski-like [8–10], meander line [11–13], Koch [14–16], Spiral shape [17], and hybrid fractal geometries [18].

A dual-band bandpass microstrip filter (DB-BPF) is proposed for RF and microwave applications. The design methodology is based on two primary principles: first, the incorporation of metamaterial C-shaped split ring resonators (C-SRRs) to achieve left-handed (LH) behavior with minimal losses, and second, the use of a microstrip line with an extended folded structure to facilitate miniaturization [2]. Additionally, a slotted conical patch antenna integrated with a small triangular patch has been developed for multiband operation, catering to both microwave and millimeter-wave applications [3]. Another study focuses on designing a multi-mode dual-band bandstop filter (MM-DBBSF), utilizing a quarter-wavelength coupled line structure to obtain highly selective dual-band bandstop responses [4].

The use of modified Minkowski fractal geometry has gained attention in microwave circuit design due to its excellent space-filling properties. This characteristic allows for the development of compact circuits, aligning with the requirements of modern communication systems that demand reduced size [8]. A compact microstrip bandpass filter (BPF) has been introduced based on a modified Minkowski fractal defected ground structure (DGS), where two coupled resonators etched with fractal geometries are used [8]. Similarly, a microstrip patch antenna employing a Minkowski-like fractal design has been studied to improve impedance matching using a $\lambda/4$ impedance converter positioned between the microstrip radiation patch and a 50 Ω feed line [9]. Additionally, a dielectric sensor incorporating a defected ground structure with a Minkowski-like fractal resonator has been proposed for estimating the complex permittivity of binary mixtures, such as ethanol-water, methanol-water, and ethanol-methanol [10]. In this design, glass capillary tubes are positioned at the center of the metamaterial, oriented perpendicular to the sensor surface.

Meander-line planar structures are widely utilized in applications that prioritize miniaturization and compactness. A circuit model analysis of a meander-line antenna has been con-

* Corresponding author: Hayder S. Ahmed (hayder.s@coeng.uobaghdad.edu.iq).

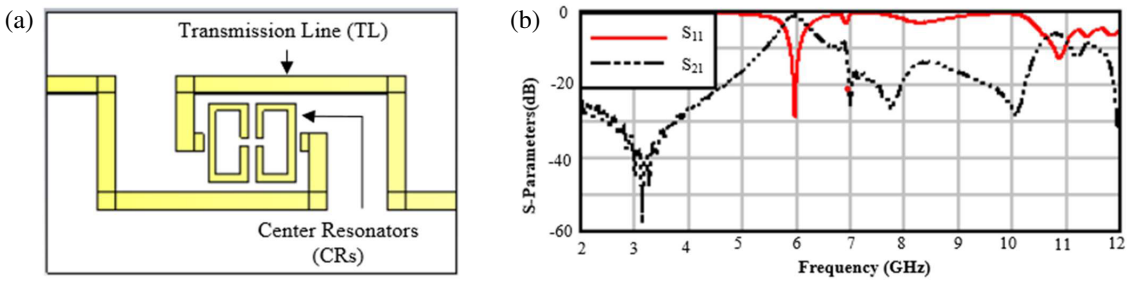

FIGURE 1. (a) The traditional DB-BPF [2]. (b) S_{11} and S_{21} of conventional DB-BPF.

ducted, enabling the accurate computation of its resonant frequency through an equivalent lumped circuit model [11]. A novel compact microstrip bandpass filter featuring a meander-line resonator has also been introduced, demonstrating a highly reduced size of approximately $\lambda_g/8 \times \lambda_g/8$ at a center frequency of 2.445 GHz [12]. The use of meander-line structures in impedance transformers has been explored, showing that while they offer narrower bandwidths than stepped-impedance transformers, they provide significantly enhanced shape factors in stripline and microwave-integrated circuit (MIC) implementations [13]. Furthermore, hybrid meander-line transformers provide circuit designers with increased flexibility in shaping transformer geometries while maintaining similar electrical performance to both stepped-impedance and meander-line transformers.

An alternative approach employs a combination of dual-mode techniques and fractal-based resonator geometries to develop a compact band-reject filter [14]. The proposed design is based on triangular patch resonators with embedded slit structures, where Koch fractal geometry is applied to the uncoupled side lengths of the triangular patch to achieve enhanced miniaturization [14]. A fractal-based dual-mode microstrip bandstop filter (BSF) has also been investigated, with size reduction achieved by applying Minkowski fractal geometry to a conventional triangular dual-mode resonator [15]. Similarly, an octagon-shaped fractal ultra-wideband multiple-input-multiple-output (MIMO) antenna has been introduced, leveraging the self-similarity and space-filling characteristics of Koch fractal geometry to achieve both miniaturization and broadband functionality [16].

Additionally, hybrid configurations of fractal-based metamaterials have been examined. A structure comprising two square split rings with spiral-shaped metallic arms has been demonstrated to exhibit unique metamaterial properties, including negative permittivity, negative permeability, and a negative refractive index, thereby enhancing surface current interactions with applied transverse electromagnetic waves [17]. Another study explores a hybrid fractal antenna, illustrating the advantages of fractal geometries in improving radiation efficiency through self-similarity and space-filling properties [18]. These characteristics play a crucial role in enabling multi-frequency resonance, making fractal-based designs highly beneficial for modern wireless communication systems.

In this work, a new compact dual-band bandpass filter (BPF) is designed for RF and microwave wireless applications, operating at center frequencies of 6 GHz and 11 GHz. The proposed design is based on two key concepts: integrating metamaterial resonators using the first iteration of a modified Minkowski fractal geometry and incorporating meander-line fractal geometry within the transmission line, which serves as both a feed and an additional resonator. The proposed technique has not been previously utilized. The filter is fabricated using a Rogers RO4003 substrate with a thickness of 1.5 mm and a dielectric constant of 3.5. The overall dimensions of the proposed structure are 23.8 mm $\times$20.6 mm. Design and performance evaluations are conducted using Computer Simulation Technology (CST) software. To validate the proposed structure, the filter was fabricated, and experimental measurements showed a high correlation with the simulated results, confirming its effectiveness for dual-band RF/microwave applications.

2. ANALYSIS OF CONVENTIONAL DUAL-BAND BPF

The conventional Dual-Band Bandpass Filter (DB-BPF), shown in Fig. 1(a), is designed based on two key concepts: the incorporation of metamaterial resonators in C-shaped split rings (C-SRR) and TLs. It is designed using a Rogers RO4003 substrate with a thickness of 1.5 mm and a dielectric constant of 3.5. The feeding transmission line has a width (W_L) of 1.4 mm and a characteristic impedance (Z_0) of 80 Ω, which is calculated using the equations provided in [19].

$$\epsilon_e = \frac{\epsilon_r + 1}{2} + \frac{\epsilon_r - 1}{2} \frac{1}{\sqrt{1 + 12h/W_L}} \tag{1}$$

$$Z_0 = \begin{cases} \frac{60}{\sqrt{\epsilon_e}} \ln\left(\frac{8h}{W_L} + \frac{W_L}{4h}\right) & \text{for } W_L/h \leq 1 \\ \frac{120\pi}{\sqrt{\epsilon_e}[W_L/h + 1.393 + 0.667 \ln(W_L/h + 1.444)]} & \text{for } W_L/h \geq 1 \end{cases} \tag{2}$$

The structure was re-simulated using CST based on the dimensions provided in [2]. As shown in Fig. 1(b), the filter exhibits two frequency bands:

- The first band appears at 11.9 GHz, with $S_{11} = -12.27$ dB and $S_{21} = -6$ dB at the center frequency.
- The second band appears at 5.9 GHz, with $S_{11} = -28.26$ dB and $S_{21} = -1$ dB.

Minor variations in S_{11} and S_{21} compared to [2] are attributed to slight differences in proximity dimensions, as illustrated in Fig. 1(b).

The structure consists of two main components:

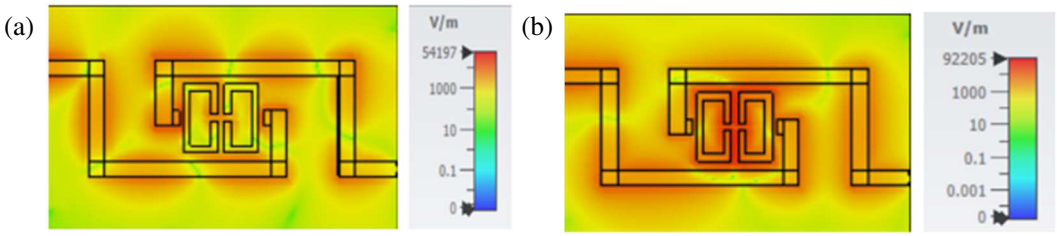

FIGURE 2. (a) E-filed distribution at 10.9 GHz. (b) E-filed distribution at 5.9 GHz.

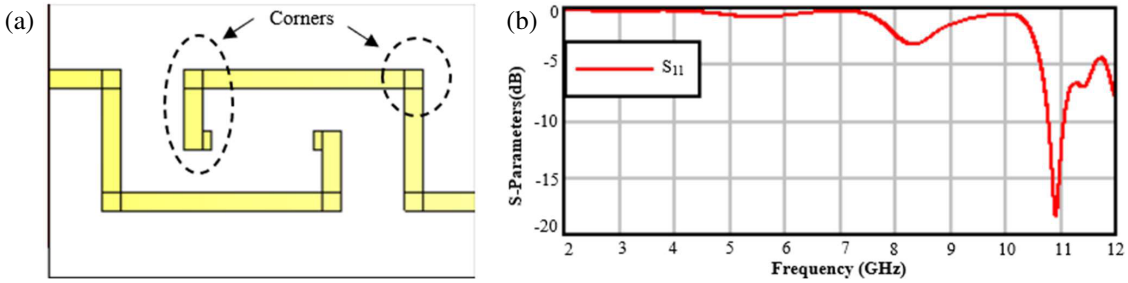

FIGURE 3. (a) Conventional BPF with TLs only. (b) S_{11} of conventional BPF with TLs only.

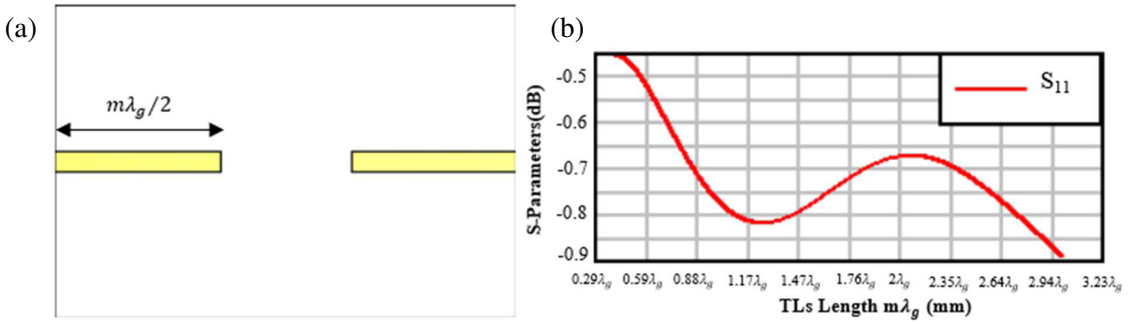

FIGURE 4. (a) The structure with straight TLs. (b) S_{11} of different lengths of $m\lambda_g/2$ at 10.9 GHz.

1. Transmission Lines (TLs)
2. Center Resonators (CRs) (Fig. 1(a))

The transmission lines act as feeds for the center resonators, generating the first mode at 10.9 GHz. As shown in Fig. 2(a), the E-field distribution at 10.9 GHz is concentrated on the TLs.

The center resonators are C-shape resonators that are constructed to produce the second mode and have a metamaterial property.

The length of TLs is equal to $2.5\lambda_g$ where λ_g is the guided wavelength that can be calculated by:

$$\lambda_g = \frac{\lambda_o}{\sqrt{\epsilon_e}} \tag{3}$$

where λ_0 is the free space wavelength, ϵ_e the effective permittivity, f the center frequency, and c the light speed. To confirm the role of the transmission lines (TLs), the structure was simulated with only TLs, as shown in Fig. 3. The results in Fig. 3(b) indicate that only one resonance appears at 10.9 GHz, while the second resonance is eliminated. The S_{11} value at 10.9 GHz is -17.9 dB, confirming that the TLs are responsible for generating the first mode.

Most researchers use $0.5\lambda_g$ to achieve resonance with compact structures, allowing multiple segments of $0.5\lambda_g$ to produce the same resonance effect. To verify this principle, the authors simulate structures with straight transmission lines of different lengths ($m\lambda_g/2$) using CST microwave studio, as shown in Fig. 4(a). From Fig. 4(b), the S_{11} values at 10.9 GHz for different lengths of straight transmission lines (TLs) range between -0.45 dB and -0.9 dB. This indicates that resonance does not occur at 10.9 GHz when using either $0.5\lambda_g$ or $2.5\lambda_g$ straight TLs, which have the same length as those in the conventional structure. Therefore, these straight TLs cannot be used to generate the mode at 10.9 GHz.

In contrast, the curved structure of the conventional design, which incorporates three corners with TLs, reduces characteristic impedance and reflection losses, enabling resonance at 10.9 GHz, as shown in Fig. 3 [20].

The second part of the conventional structure consists of center resonators (CRs), which are open-loop resonators, as

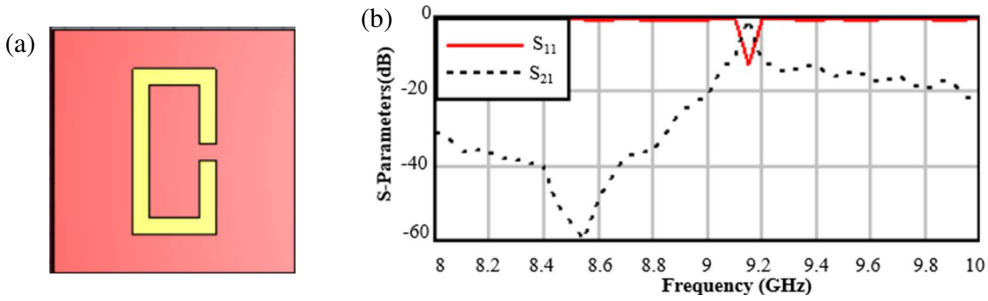

FIGURE 5. (a) CRs unit cell, (b) S-parameters of it.

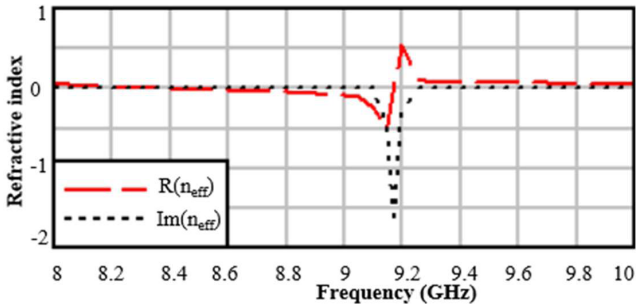

FIGURE 6. Extracted real part and imaginary part of Refractive index of the CRs.

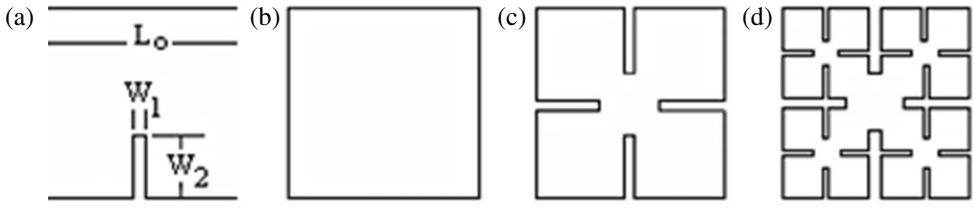

FIGURE 7. The Minkowski fractal geometry: (a) the generator, (b), (c) and (d) represent the zero, the 1st, and the 2nd iteration levels respectively [8] and [10].

shown in Fig. 1(a). According to [1], these resonators exhibit metamaterial properties. The unit cell was re-simulated using CST with a Rogers RO4003 substrate, featuring a thickness of $h = 1.5$ mm and a dielectric constant of 3.5. The overall unit cell size is 8.8 mm $\times$8.8 mm, as shown in Fig. 5, along with its corresponding S-parameters.

The effective parameters of the CRs are extracted using the Nicolson-Ross-Weir (NRW) method [21,22], and the refractive index of the C-SRR (Split Ring Resonator) is given by Eq. (4) [23].

$$n_{eff} = \frac{c}{j\pi fh} \times \sqrt{\left[\frac{1-(S_{21}+S_{11})}{1+(S_{21}+S_{11})}\right]\left[\frac{1-(S_{21}-S_{11})}{1+(S_{21}-S_{11})}\right]} \quad (4)$$

From the imaginary and real parts of the refractive index shown in Fig. 6, the CRs have negative values (simultaneously) in the frequency range around the resonance of 9.17 GHz. This characteristic can justify the LH electromagnetic behavior of the proposed metamaterial resonator [2].

Figure 2(b) presents the E-field distribution at 5.9 GHz, where the E-field is concentrated on the CRs, indicating that they generate the second mode. The length of each resonator is $0.5\lambda_g$.

3. METHODOLOGY

Fractal geometry is used to design a miniaturized dual-band filter proposed by [2] by adding a resonator with the 1st iteration. Modified-Minkowski fractal geometry with added iterations is applied on an open-loop rectangle resonator to achieve miniaturization.

The common modified-Minkowski geometries with different iterations Zero [8–10], 1st, and 2nd are shown in Fig. 7, respectively.

The perimeter P_n of the nth iteration is given by [8] and [10]

$$P_n = \left(1 + \frac{2w_2}{L_o}\right) P_{n-1} \quad (5)$$

where w_2 and L_o are as shown in Fig. 7. Eq. (5) implies that, as n approaches infinity, the perimeter goes to infinity.

The objective of using fractal geometry is to increase the surface current path length. Consequently, a reduced resonant fre-

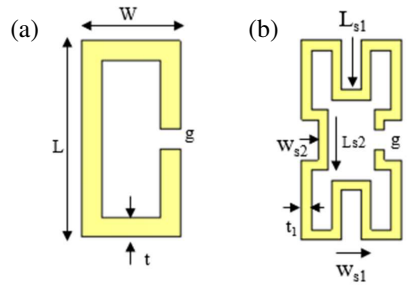

FIGURE 8. (a) Rectangle open loop resonator with zero iteration. (b) Rectangle open loop resonator with modify-Minkowski 1st iteration.

quency or a reduced resonator size should be considered if the design frequency is to be maintained [8, 10].

Figure 8 illustrates the application of the modify-Minkowski technique to rectangular open-loop resonators at both the zero and first iterations. The outer dimensions of these resonators remain consistent at $L \times W$ for both iterations. Consequently, this study utilizes rectangular open-loop resonators at the first iteration to design a dual-band BPF.

The perimeter P_n of the nth iteration of rectangle resonators without the gap "g" is given by

$$P_n = \left(1 + \frac{2L_{s1}}{W} + \frac{2w_{s2}}{L}\right) P_{n-1} \tag{6}$$

where W, w_{s2}, L, L_{s1} are as shown in Fig. 8. Eq. (6) implies that, as n approaches infinity, the perimeter goes to infinity. The perimeter of the open loop rectangle with modify-Minkowski resonator for the nth iteration is given by:

$$L_n = p_n - g \tag{7}$$

4. MEANDER LINE FRACTAL GEOMETRY

Meanders are combinatorial structures with a topological nature, capturing the relationship between planarity and connectedness. They represent systems formed by the intersections of two curves in a plane, with equivalence considered up to homeomorphism within the plane [24].

A meander consists of two distinct simple planar curves. In a geographical analogy, these curves can be thought of as a river and a road. The two curves intersect a finite number of times, with these crossings accounting for all interactions between them. As illustrated in Fig. 9, a meander with $m = 7$ has seven intersections, where m represents the order of the meander.

FIGURE 9. An open meander represented as a river and a road.

Meanders can be classified into four types: Open Meander, Closed Meander, Arch Configuration, and Semi-Meander. In this paper, an Open Meander is utilized to design a compact dual-band bandpass filter (BPF) by extending the current path in the transmission lines (TLs).

An Open Meander consists of an oriented simple curve and a line in the plane, which crosses a finite number of times and intersects only transversally. Two open meanders are considered equivalent if there exists a homeomorphism of the plane that maps one meander onto the other [24].

5. PROPOSED DESIGN OF DUAL-BAND BPF

A compact DB-BPF design has been passed through four stages. Firstly, a 1st iteration of modify-Minkowski fractal geometry applied on the CRs as shown in Fig. 10(a) is the first stage.

The first-stage BPF was designed using a Rogers RO4003 substrate with a thickness of 1.5 mm and a dielectric constant of 3.5. The overall size of the proposed filter is 32.2 mm $\times$20.6 mm.

To simulate the proposed BPF, CST was used, as shown in Fig. 10, with a flat copper ground plane. The feeding transmission line width (W_L) was 1.4 mm, with a characteristic impedance (Z_0) of 80 Ω. However, the authors considered the waveguide port constant to match the input and output impedance of 50 Ω, simulating practical conditions. Consequently, a small mismatch between the transmission lines (TLs) and the input/output ports is expected.

All dimensions of the proposed structure are listed in Table 1.

TABLE 1. Dimension of 1st stage BPF.

Parameters	Value (mm)	Parameters	Value (mm)
Width	32.2	Length	20.6
W_L	1.4	L_{F1}	5.4
L_{F2}	9.2	L_{F3}	18
L_{F4}	6	z	0.6
L_g	7.6	L	6.24
g	0.624	W	3.12
L_{s1}	1.5	L_{s2}	1.8
W_{s1}	0.6	W_{s2}	0.5
t_1	0.3		

As shown in Fig. 10(b), the first mode appeared at 10.89 GHz with S_{11} equal to -10.4 dB, S_{21} equal to -4.6 dB, and bandwidth 100 MHz while the second mode shifted down to 5.6 GHz with S_{11} equal to -26 dB, S_{21} equal to -1.3 dB, and bandwidth 48 MHz. The first mode stays near 11 GHz while the second one shifted down about 400 MHz by only applying 1st modify-Minkowski with the same dimensions of CRs in the conventional BPF. The insertion loss of the first mode is high because of the mismatch between the TLs characterized impedance and port impedance.

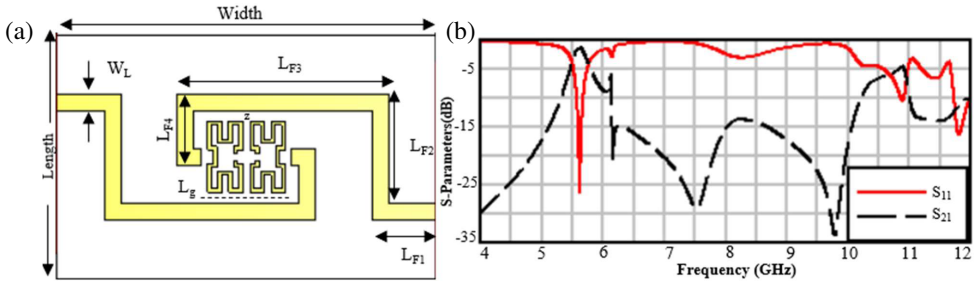

FIGURE 10. BPF in the first stage. S-parameters of first stage BPF.

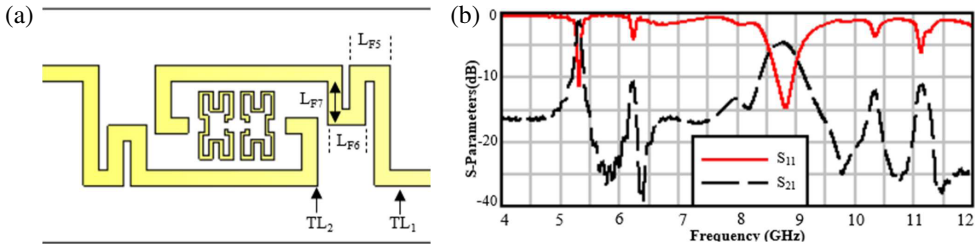

FIGURE 11. (a) Second stage BPF structure. (b) S-parameters of it.

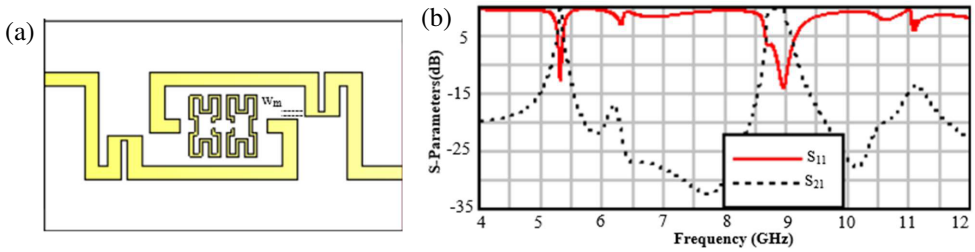

FIGURE 12. (a) Structure of the third stage BPF. (b) S-parameters of it.

In the second stage, open meander line fractal geometry with $m = 2$ has been applied on the TLs to increase the length of the current path. The gap between Transmission Line one, TL1, and Transmission line two, TL2, is an important factor that restricted the dimensions of the mender line to avoid the coupling between the TLs, as shown in Fig. 11(a) which are $L_{F5} = 3.6$ mm, $L_{F6} = 3.4$ mm and $L_{F7} = 3.9$ mm. The S-parameters of the second stage BPF are shown in Fig. 11(b).

From S-parameters in Fig. 12(b), the first mode produced by TLs has been shifted down to 8.8 GHz with S_{11} equal to -14.7 dB, S_{21} equal to -4 dB, and bandwidth 272 MHz while the second mode has some shift to 5.3 GHz with S_{11} equal to -11.23 dB, S_{21} equal to -3 dB, and bandwidth 22 MHz. The insertion loss of the first mode has not been improved while the insertion loss of the second mode increased to -3 dB because the meander line of one TL became so close to the second TL. Thirdly, the step impedance technique has been used with the horizontal arm of the meander line to improve the insertion loss of both modes. CST optimizer has been used to find the best value to width of the horizontal arm of the meander line that is $W_m = 0.5$ mm as shown in Fig. 12 with the third stage BPF.

From the S-parameters of the third-stage BPF shown in Fig. 12(b), the losses of insertion for both modes have been improved. The first mode exhibits an S_{21} value of -0.14 dB, while the second mode achieves an S_{21} of -0.08 dB. Although the third-stage BPF retains the same dimensions as the conventional BPF, its center frequencies are shifted downward.

Lastly, the dimensions of the third-stage BPF have been adjusted to obtain center frequencies of 6 GHz and 11 GHz. The proposed compact dual-band BPF, representing the fourth and final stage, has been simulated using CST, as illustrated in Fig. 13. The updated dimensions are provided in Table 2.

Figure 13(b) shows the S-parameters of the compact proposed DB-BPF. From the S-parameters, the first mode is at 11.02 GHz with S_{11} equal to -13.9 dB, S_{21} equal to -0.28 dB, and bandwith 25 MHz while the second mode is at center frequency 6.02 GHz with S_{11} equal to -20.1 dB, S_{21} equal to -0.5 dB, and bandwidth 310 MHz. The overall size of the proposed BPF is 23.8 mm $\times$ 20.6 mm. The miniaturization has been achieved with 26%. It can be miniaturized more, but this miniaturization percentage is to keep the center frequencies of the reference design of [1]. The E-field distribution at first mode 11.02 GHz focused at TLs and at second mode 6.02 GHz on the 1st iteration modify-Minkowski fractal geometry resonators, shown in Fig. 14.

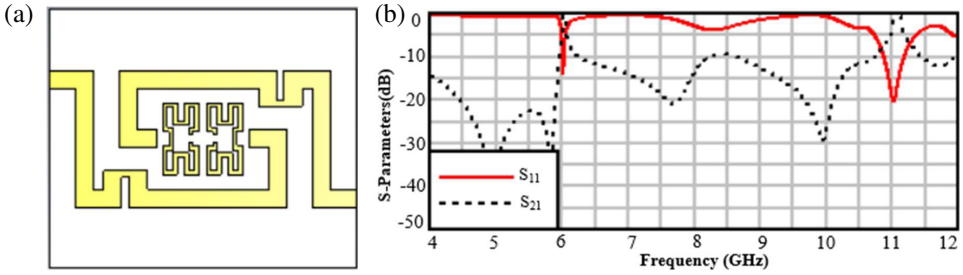

FIGURE 13. (a) The fourth stage BPF. (b) Its S-parameters.

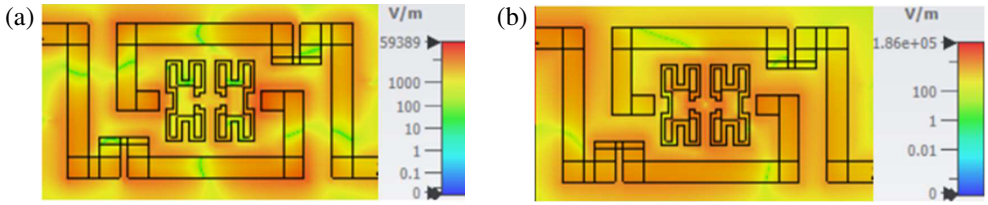

FIGURE 14. (a) E-field distribution at 11.02 GHz. (b) E-field distribution at 6.02 GHz.

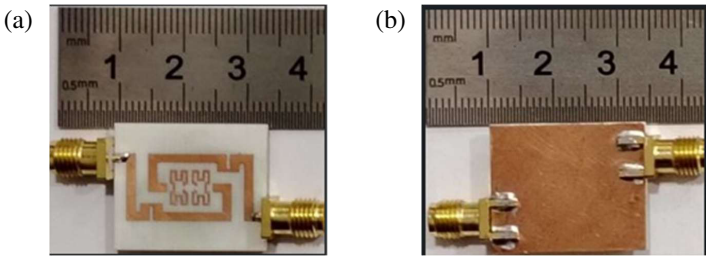

FIGURE 15. Fabrication of the proposed compact dual-band BPF. (a) Top view. (b) Bottom view.

6. FABRICATION DUAL-BANDS BPF

To validate the performance of the proposed compact dual-band bandpass filter (BPF), the design was fabricated using a ProtoMat S100, as illustrated in Fig. 15. Fig. 15(a) presents the top view of the fabricated filter. In contrast, Fig. 15(b) displays the bottom view, which features a flat copper ground plane. The filter was implemented on a Rogers RO4003 substrate with a thickness of 1.5 mm and a dielectric constant of 3.5. The final fabricated structure has overall dimensions of 23.8 mm $\times$ 20.6 mm. The detailed design parameters are provided in Table 2.

TABLE 2. Dimensions of the proposed dual-band BPF.

Parameters	Value (mm)	Parameters	Value (mm)
Width	238	Length	20.6
W_L	1.4	L_{F1}	3.4
L_{F2}	9.2	L_{F3}	16.4
L_{F4}	6	z	0.6
L_g	7.2	L	5.57
g	0.55	W	2.78
L_{s1}	1.39	L_{s2}	1.74
W_{s1}	0.55	W_{s2}	0.46
t_1	0.3	L_{F5}	3.6
L_{F6}	3.4	L_{F7}	1.4

7. RESULTS AND MEASUREMENTS

The S-parameters and input impedance of the proposed dual-band BPF were measured using an Anritsu MS4642A Vector Network Analyzer (VNA). The measurement of the parameters is shown in Fig. 16 and Fig. 17. As illustrated in Fig. 15(b), there is a strong correlation between the measurement and simulation results. The measured S_{11} values are -18.7 dB at 11.02 GHz and -12 dB at 6.02 GHz, while the measured S_{21} values are -0.29 dB at 11.02 GHz and -0.25 dB at 6.02 GHz. The bandwidth of each band is 200 MHz at the center frequency of 11.02 GHz and 20 MHz at the second center frequency of 6.02 GHz. The discrepancies between the measurements and simulations are attributed to fabrication conditions, welding effects, and measurement accuracy. Fig. 17 also presents the measured real (Re) and imaginary (Im) components of the input impedance. The real part of the input impedance is 53 Ω at 11.02 GHz and 45 Ω at 6.02 GHz. The step impedance technique enhances the total input impedance of the transmission lines (TLs), bringing it closer to the input port impedance. As a result, insertion loss is reduced, as confirmed by both simulation and measurement results.

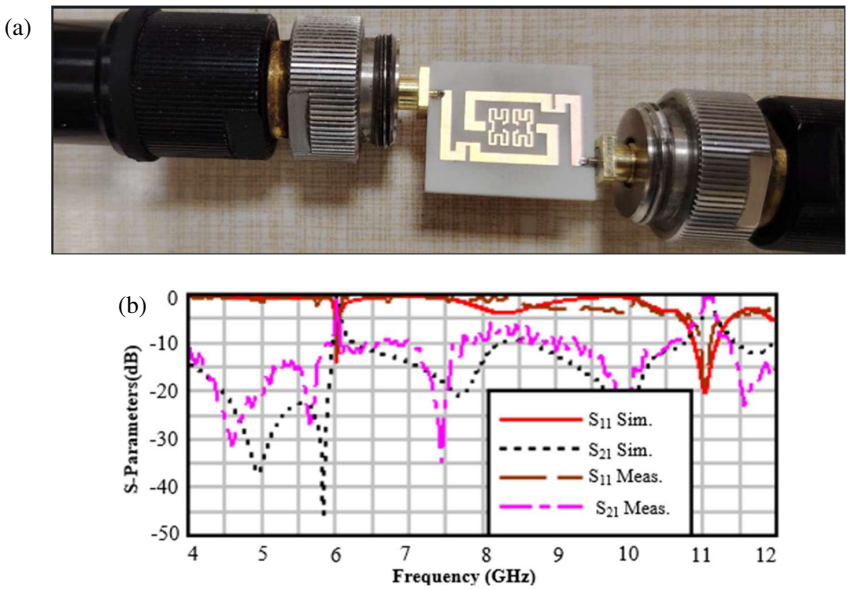

FIGURE 16. (a) The proposed Compact Dual-Band filter on VNA. (b) The S-parameters measurements and simulation.

TABLE 3. Comparison between the proposed compact dual-band BPF and the dual-band planer structure.

	Overall size $\lambda_g \times \lambda_g$	Insertion loss (dB)	Frequency (GHz)	Layer	Fabrication
Reference [2]	1.05×0.67	1.02/0.65	11-6	Single	NA
Reference [5]	0.31 ×0.46	0.5/0.77	1.9/1.25	Two	Yes
Reference [6]	1.56×—	0.8/1.02	5.4/4.6	Single	Yes
Reference [7]	–	0.84/0.25	2.89/1.11	Three	Yes
Proposed work	0.75×0.67	0.29/0.25	11/6	Single	Yes

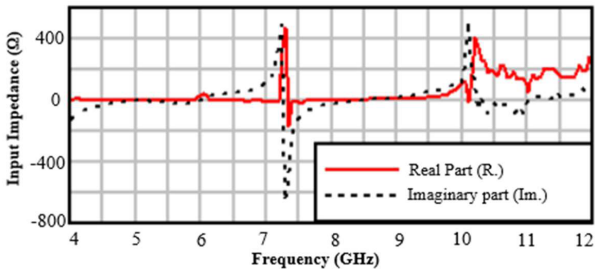

FIGURE 17. Measurements input impedance of the proposed filter.

As shown in Table 3, the proposed structure is smaller than other dual-band planer structures with transmission lines to feed, except for [5] because it consists of two layers that make the design and fabrication more complex. Also, the proposed work achieves less insertion loss than previous works. The proposed structure achieves 26% miniaturization in size, and the simulation results are correlated with those measured after fabrication.

Notably, while further size reduction is possible, the authors maintained the center frequencies at 6 GHz and 11 GHz, as in [2], to facilitate comparison for the reader. However, the meander-line structure has a limitation: increasing its length results in greater coupling with adjacent transmission lines. Additionally, using an alternative fractal geometry, such as the Piano fractal, could be more beneficial.

8. CONCLUSION

In this paper, a compact dual-band bandpass filter (BPF) is proposed and designed based on two key concepts. First, the transmission lines (TLs) serve as feeders for the center resonators (CRs), resonating at an upper frequency of 11 GHz. Meanwhile, the CRs, which exhibit metamaterial properties, resonate at 6 GHz for RF/microwave applications. To achieve miniaturization, two different fractal geometries are applied: a first-iteration modified-Minkowski fractal geometry on the CRs and a second-order meander-line fractal geometry on the TLs. The proposed structure is designed using a Rogers RO4003 substrate with a thickness of 1.5 mm and a dielectric constant of 3.5. Simulations are conducted using CST Microwave Studio, and the fabricated dual-band BPF demonstrates strong agreement with the simulation results. The measured return losses (S_{11}) are -18.7 dB at 11.02 GHz and -12 dB at 6.02 GHz, while the insertion losses (S_{21}) are -0.29 dB and -0.25 dB at the respective frequencies. The filter achieves bandwidths of 200 MHz at 11.02 GHz and 20 MHz at 6.02 GHz. The size of the proposed BPF is 23.8 mm × 20.6 mm which achieves 26% reduction.

REFERENCES

[1] Federal Communications Commission, "FCC opens entire 6 GHz band to very low power device operations," [Online]. Available: https://docs.fcc.gov/public/attachments/DOC-408129A1.pdf. [Accessed: Apr. 2, 2025], Dec. 2024.

[2] Berka, M., T. Islam, S. Das, A. Serhane, M. L. Kumar, and Z. Mahdjoub, "Design of miniaturized dual-band bandpass microstrip filter based on C-shaped metamaterial resonators for RF/microwave applications," *J. Nano- Electron. Phys.*, Vol. 16, No. 4, 04012, 2024.

[3] Khan, Z., M. H. Memon, S. U. Rahman, M. Sajjad, F. Lin, and L. Sun, "A single-fed multiband antenna for WLAN and 5G applications," *Sensors*, Vol. 20, No. 21, 6332, 2020.

[4] Faisal, M., S. Khalid, M. U. Rehman, and M. A. Rehman, "Synthesis and design of highly selective multi-mode dual-band bandstop filter," *IEEE Access*, Vol. 9, 43 316–43 323, 2021.

[5] Abdel-Aziz, M., A. S. A. El-Hameed, A. A. Awamry, and A. S. Mohra, "Dual-band broadside-coupled based BPF with improved performance," *AEU — International Journal of Electronics and Communications*, Vol. 138, 153895, 2021.

[6] Riaz, M., B. S. Virdee, P. Shukla, K. Ouazzane, M. Onadim, and S. Salekzamankhani, "Quasi-elliptic dual-band planar BPF with high-selectivity and high inter-band isolation for 5G communications systems," *Microwave and Optical Technology Letters*, Vol. 62, No. 4, 1509–1515, 2020.

[7] Yang, L., M. Malki, and R. Gómez-García, "Multilayer dual-band bandpass filter using microstrip-to-slotline transitions and transversal signal-interference microstrip lines," in *2024 IEEE Radio and Wireless Symposium (RWS)*, San Antonio, TX, USA, Jan. 2024.

[8] Ali, J. K. and H. T. Ziboon, "Design of compact bandpass filters based on fractal defected ground structure (DGS) resonators," *Indian Journal of Science and Technology*, Vol. 9, No. 39, 1–9, 2016.

[9] Qin, F., J. Lei, and B. Ren, "Compact microstrip antenna based on minkowski-like sided fractal," in *2021 IEEE International Conference on Power Electronics, Computer Applications (ICPECA)*, 940–943, Shenyang, China, Jan. 2021.

[10] Gulsu, M. S., F. Bagci, S. Can, A. E. Yilmaz, and B. Akaoglu, "Minkowski-like fractal resonator-based dielectric sensor for estimating the complex permittivity of binary mixtures of ethanol, methanol and water," *Sensors and Actuators A: Physical*, Vol. 330, 112841, 2021.

[11] Das, A., S. Dhar, and B. Gupta, "Lumped circuit model analysis of meander line antennas," in *2011 11th Mediterranean Microwave Symposium (MMS)*, 21–24, Yasmine Hammamet, Tunisia, Sep. 2011.

[12] Qing, X. M., Y. W. M. Chia, and J. Sun, "A novel miniaturized microstrip bandpass filter using a meander-line resonator," *Microwave and Optical Technology Letters*, Vol. 32, No. 4, 319–321, 2002.

[13] Cristal, E. G., "Meander-line and hybrid meander-line transformers," *IEEE Transactions on Microwave Theory and Techniques*, Vol. 21, No. 2, 69–76, Feb. 1973.

[14] Ahmed, H. S., A. J. Salim, M. R. Hussan, H. A. Hammas, M. T. Yassen, S. Mutashar, and J. K. Ali, "Design of compact dual-mode fractal based microstrip band reject filter," *ARPN Journal of Engineering and Applied Sciences*, Vol. 13, No. 7, 2395–2399, 2018.

[15] Ahmed, H. S., A. J. Salim, J. K. Ali, and M. A. Alqaisy, "A fractal-based dual-mode microstrip bandstop filter for wireless applications," in *2016 16th Mediterranean Microwave Symposium (MMS)*, 1–4, Abu Dhabi, United Arab Emirates, Nov. 2016.

[16] Tripathi, S., A. Mohan, and S. Yadav, "A compact Koch fractal UWB MIMO antenna with WLAN band-rejection," *IEEE Antennas and Wireless Propagation Letters*, Vol. 14, 1565–1568, 2015.

[17] Siddiky, A. M., M. R. I. Faruque, S. Abdullah, M. T. Islam, M. U. Khandaker, and K. S. Al-Mugren, "Dual square split ring enclosed spiral shaped hybrid metamaterial resonator with size miniaturisation for microwave wireless applications," *Scientific Reports*, Vol. 12, No. 1, 8028, 2022.

[18] Sharma, N., S. Kaur, and B. S. Dhaliwal, "A new triple band hybrid fractal boundary antenna," in *2016 IEEE International Conference on Recent Trends in Electronics, Information & Communication Technology (RTEICT)*, 874–878, Bangalore, India, May 2016.

[19] Pozar, D. M., *Microwave Engineering*, Fourth Editions, University of Massachusetts at Amherst, John Wiley & Sons, Inc, 2012.

[20] Thomann, W., B. Isele, and P. Russer, "Characterization of a 90 degrees curved microstrip transmission line in the time-domain and frequency-domain with 3D-TLM-method and measurements," in *IEEE Antennas and Propagation Society International Symposium 1992 Digest*, 658–661, Chicago, IL, USA, Jun. 1992.

[21] Nicolson, A. M. and G. F. Ross, "Measurement of the intrinsic properties of materials by time-domain techniques," *IEEE Transactions on Instrumentation and Measurement*, Vol. 19, No. 4, 377–382, 1970.

[22] Weir, W. B., "Automatic measurement of complex dielectric constant and permeability at microwave frequencies," *Proceedings of the IEEE*, Vol. 62, No. 1, 33–36, 1974.

[23] Sharma, S. and R. Mehra, "Printed monopole slot antenna inspired by metamaterial unit cell for wireless applications," in *Optical and Wireless Technologies*, 413–424, Sep. 2022.

[24] La Croix, M., "Approaches to the enumerative theory of meanders," University of Waterloo, 2003.